The black hole mass metallicity relation and insights into galaxy quenching

William M. Baker[1,2*], Roberto Maiolino[1,2,3], Asa F. L. Bluck[4], Francesco Belfiore[5], Mirko Curti[1,2,6], Francesco D'Eugenio[1,2], Joanna M. Piotrowska[1,2,7], Sandro Tacchella[1,2], James A. A. Trussler[8]

[1]Kavli Institute for Cosmology, University of Cambridge, Madingley Road, Cambridge, CB3 OHA, UK.
[2]Cavendish Laboratory - Astrophysics Group, University of Cambridge, 19 JJ Thomson Avenue, Cambridge, CB3 OHE, UK.
[3]Department of Physics and Astronomy, University College London, Gower Street, London WC1E 6BT, UK.
[4]Department of Physics, Florida International University, 11200 SW 8th Street, Miami, FL, USA.
[5]INAF— Osservatorio Astrofisico di Arcetri, Largo E. Fermi 5, I-50125, Florence, Italy.
[6]European Southern Observatory, Karl-Schwarzschild-Strasse 2, D-85748 Garching bei Muenchen, Germany.
[7]Cahill Center for Astronomy and Astrophysics, California Institute of Technology, Pasadena, CA 91125, USA.
[8]Jodrell Bank Centre for Astrophysics, University of Manchester, Oxford Road, Manchester M13 9PL, UK.

*Corresponding author(s). E-mail(s): wb308@cam.ac.uk;

Abstract

One of the most important questions in astrophysics is what causes galaxies to stop forming stars. Previous studies have shown a tight link between quiescence and black hole mass. Other studies have revealed that quiescence is also associated with 'starvation', the halting of gas inflows, which results in the remaining gas being used up rapidly by star formation and in rapid chemical enrichment. In this work we find the final missing link between these two findings. Using a

large sample of galaxies, we uncover the intrinsic dependencies of the stellar metallicity on galaxy properties. In the case of the star-forming galaxies, the stellar metallicity is driven by stellar mass. However, for passive galaxies the stellar metallicity is primarily driven by the black hole mass, as traced by velocity dispersion. This result finally reveals the connection between previous studies, where the integrated effect of black hole feedback prevents gas inflows, starving the galaxy, which is seen by the rapid increase in the stellar metallicity, leading to the galaxy becoming passive.

Keywords: Galaxies: abundances, Galaxies: evolution, Galaxies: stellar content, Galaxies: black holes, Galaxies: passive

Introduction

The chemical enrichment of galaxies is a powerful proxy of their history of star formation and of the evolutionary processes and mechanisms that have shaped them. This chemical enrichment is traced by the 'metallicity', the ratio of heavier elements to the Hydrogen and Helium content of either gas or stars. Metals are produced by stellar nucleosynthesis are then released via supernovae explosions and stellar winds, hence increasing the metallicity of the ISM [1]. However, the metallicity also traces other processes, such as inflows of low-metallcity gas (causing metal dilution) and outflows (often metal loaded [2, 3]).

Depending on the galaxy type and on the available data, the metallicity in galaxies can be measured for the gas-phase of the ISM, and for the stellar population. Both of these metallicities follow well known scaling relations with other galactic properties. Specifically, the metallicity is known to increase with the stellar mass of a galaxy, up until $M_* = 10^{10.5} M_\odot$ where it starts to plateau, in a relationship known as the mass-metallicity relation (MZR, [1, 4, 5]). At fixed mass the metallicity is also observed to decrease with increasing star-formation rate (i.e. anti-correlate), leading to an overall three-dimensional relationship between the quantities, known as the Fundamental Metallicity Relation (FMR, [6–8]).

The advantage of studying stellar metallicities is that they can be estimated for both star-forming and passive galaxies, whereas, due to being calculated from emission lines, gas-phase metallicities can only accurately be obtained for star-forming galaxies (although see also [9]). Star-forming galaxies and passive galaxies show large differences in stellar metallicity with passive galaxies having larger values at a given stellar mass [10–12]. This is also seen as a continuous sequence in [8], where galaxies with the lower SFR (i.e. more passive) have higher stellar metallicity. This trend is interpreted as quenching via starvation, where galaxies quench because their gas supply (via inflows) is cut off [10, 11]. Starvation implies that the remaining gas of the galaxy is converted into stars in a closed-box manner, resulting in the metallicity rising steeply because it is not diluted from accreting (low-metallicity) gas. However, even if starvation is identified as playing a key role in galaxy quenching, its causes could not be identified based solely on the metallicity analysis.

Many different causes for the quenching of star-formation have been proposed in the past, such as, AGN feedback, morphological quenching, cosmic rays, magnetic fields, and environmental effects [13]. Of particular interest, are the recent results of [14–16] where they find that the strongest link to quenching in a galaxy is the mass of the supermassive black hole at the centre (this applies for central galaxies or massive satellites). This has led [15] to conclude that it is the integrated effect of black hole accretion feedback that causes quenching. The proposed scenario, also supported by simulations [14], is that black hole accretion heats the circum-galactic medium (via radio-jets or outflows) hence preventing accretion of cold gas, and resulting in delayed quenching via starvation.

A key difficulty when investigating relationships between quantities that could cause quenching is that many of them are inter-correlated, hence correlation between quiescence and some galaxy properties does not necessarily imply causation. In the recent works discussed above [14–16] this issue was tackled by using machine learning (random forest) and partial correlation techniques, to identify direct and primary connections from indirect relations induced by spurious connections resulting from the fact that most galactic properties are intercorrelated. The same issue applies also for the metallicity scaling relations: it is hard to separate intrinsic fundamental relationships from secondary relations resulting from indirect byproducts. Within this context [7, 17–19] utilised multiple techniques to break these inter-correlations and determine the fundamental dependencies of gas-phase metallicities and other scaling relations.

In this paper we extend those studies to explore the intrinsic dependence of *stellar* metallicity as a function of galactic properties, finding the final connection between the mechanism of quenching, starvation, and the cause, integrated black hole feedback.

Definition of the sample

To investigate the dependencies of the stellar metallicity on galaxy parameters, we use galaxies from the Sloan Digital Sky Survey (SDSS) data release 7 [20], with data on their stellar masses, star-formation rates, stellar metallicities, halo masses, overdensities and velocity dispersions (for more details see Methods section 1.1). To ensure reliable stellar metallicity measurements, we employ a strict median signal to noise cut of 20 per spectral pixel [as in 11]. We also limit the sample to those galaxies with reliable redshifts in the range $0.02 \leq z \leq 0.085$ to both reduce aperture effects (i.e. the projected size of the SDSS fibre should be larger than 1 kpc) and reduce the effects of cosmological evolution [again, as in 11].

We divide our sample of galaxies into star-forming and passive based on their distance from the main sequence (using the MS definition of [21]). Star-forming galaxies are those with $\Delta\mathrm{MS} \geq -0.75$, whilst passive galaxies are those with $\Delta\mathrm{MS} \leq -0.75$. This gives us 16505 star-forming galaxies and 37241 passive galaxies.

Our primary analysis tool is random forest (RF) regression, a supervised machine learning algorithm that utilises the power of many different decision trees to accurately and simultaneously assess the contribution of several parameters in determining a target feature. In this case the target feature is the stellar metallicity of a galaxy. The parameters that we explore are: stellar mass (M_*), star formation rate (SFR),

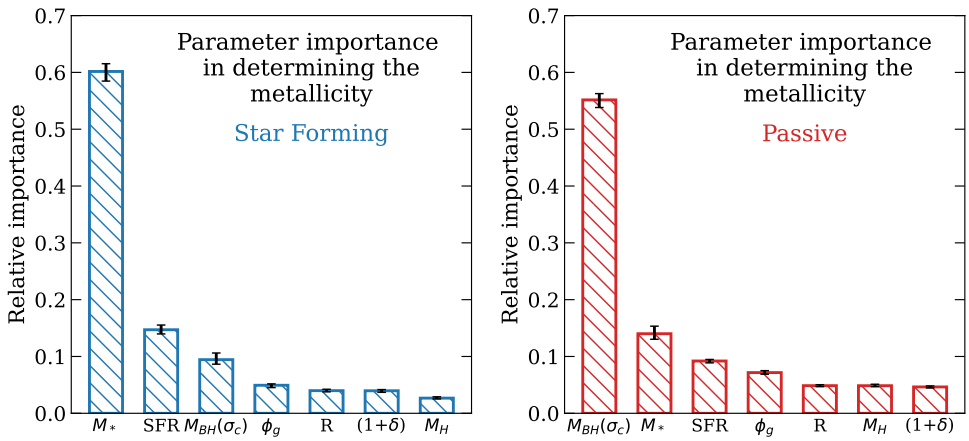

Fig. 1 The importance of various galactic properties in determining the stellar metallicity (Z) for star-forming (left panel) and passive (right panel) galaxies. The galactic parameters evaluated are: the stellar mass (M_*), the star formation rate (SFR), the black hole mass ($M_{\rm BH}(\sigma_c)$, as inferred from the central velocity dispersion), the gravitational potential (traced by $\phi_g = M_*/r_e$), a control uniform random variable (R), the overdensity of galaxies ($1+\delta$), and the halo mass (M_H). The left hand panel shows that for star-forming galaxies the primary dependence of stellar metallicity is on stellar mass via the mass-metallicity relation (MZR). However, for passive galaxies (right hand panel) the stellar metallicity dependence is almost purely on black hole mass.

the gravitational potential as approximately traced by $\Phi_g = M_*/R_e$, where R_e is the circularized half-light radius in the r-band, the mass of the dark matter halo (M_H) and the strength of the overdensity of galaxies ($1+\delta$). Among the parameters we also include the central black hole mass as traced by the central velocity dispersion ($M_{\rm BH} = M_{\rm BH}(\sigma_c)$). Various authors have shown that the central velocity dispersion is tightly linked to the central black hole mass [14, 22], although we note that the central velocity dispersion might correlate with the dynamical mass or gravitational potential. However, later on we will discuss (and exclude) that neither dynamical mass nor gravitational potential play a role in determining the stellar metallicity. Finally, we also include a uniform random variable as a control. Summarising, with our analysis we can explore whether the stellar metallicity depends on internal properties of the individual galaxy (e.g. stellar mass, black hole mass, SFR) or environmental properties (e.g. halo mass, overdensity strength). We apply the random forest regression separately to our star forming and passive samples. For each of these, half the sample is used to train the random forest while the other half is used to test the predictions.

The key parameters according to Random Forest regression

Fig. 1 is a bar-chart showing the relative importance of the various quantities in determining the stellar metallicities, as inferred from the random forest analysis, for star-forming galaxies (left panel, blue) and passive galaxies (right panel, red). For the star-forming galaxies, the stellar metallicity is primarily driven by stellar mass (i.e. the MZR) with a secondary contribution from the SFR (i.e. the FMR, as in [8]). However, for passive galaxies the stellar metallicity is primarily driven by the black hole mass (as

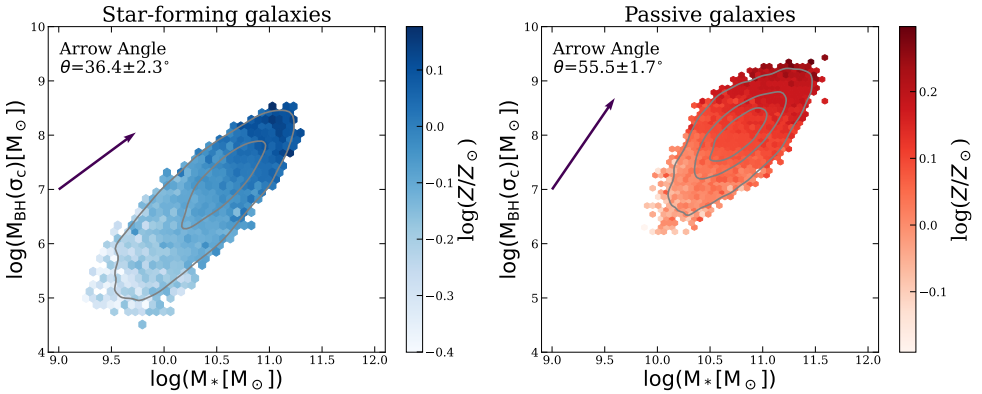

Fig. 2 Black hole mass versus stellar mass colour coded by median stellar metallicity for star-forming galaxies (left panel) and passive galaxies (right panel). The arrow angle points in the direction of the greatest increasing gradient of the stellar metallicity (i.e. it quantifies the colour-shading). The arrows and colour-shading gradients show that, in the left panel for star-forming galaxies, increasing stellar metallicity is linked to increasing stellar mass (i.e. the arrow angle is closer to the horizontal), whilst in the right panel for passive galaxies, the stellar metallicity is linked more to increasing black hole mass (the arrow angle is closer to vertical than horizontal). This means that star-forming galaxies' stellar metallicity shows a stronger dependence on stellar mass than black hole mass, whilst for passive galaxies this is reversed.

traced by σ_c) with a small secondary importance on M_* and SFR. Hence, the relative importance between stellar mass and black hole mass *swap* depending on whether the galaxies are star-forming or passive.

One key aspect to note is that we see little to no dependence on $\Phi_g = M_*/R_e$, which is a proxy of the gravitational potential - this indicates the importance of black hole mass as traced by σ_c is not simply linked to the gravitational potential instead. Additionally, later on we use two smaller samples, but with spatially resolved spectroscopic information from the MaNGA survey [23], for which the dynamical masses and gravitational potential could be estimated accurately. That analysis will show that neither the dynamical mass nor the gravitational potential of the galaxy drive the stellar metallicity, while also in that sample, black hole mass is the primary driver.

Finally, Fig. 1 shows that there is no significant dependence of the stellar metallicity on environment (M_H or $(1+\delta)$), for either the star-forming or passive galaxies. In the Methods section we also verify that this result holds also when separating the sample between central and satellite galaxies.

Direction of the relationship - partial correlation coefficients

We next investigate more visually the observed dependence of stellar metallicity on stellar and black hole mass in star-forming and passive galaxies, respectively, by reducing the dimensionality of the problem, specifically using 'simple' 3D diagrams [24], which also allow us to assess the sign of the relation, i.e. whether positive or negative, which is not possible via the random forest. Figure 2 shows black hole mass (as traced by σ_c) versus stellar mass, colour-coded by the median stellar metallicity in

each bin for star-forming galaxies (left panel) and passive galaxies (right panel). Contours show the underlying density distribution of galaxies, where each outer density contour encloses 90% of the galaxy population. The arrow angle shows the direction of the steepest metallicity gradient (i.e. following the colour shading) and is calculated (from the horizontal) by the ratio of the partial correlation coefficients between the stellar metallicity, stellar mass and black hole mass. The left panel shows that both the arrow and the colour-shading follow the stellar mass (x axis) more than the black hole mass (y axis) meaning that the primary driver in increasing the stellar metallicity of star-forming galaxies is the stellar mass. However, the right panel shows the opposite, where the stellar metallicity gradient traced by arrow and color shading follow more closely the black hole mass (y axis) than stellar mass (x axis). This confirms the result of the random forest in a more visual way. More importantly, these diagrams provide the direction of this correlation, i.e. for passive galaxies the greater the black hole mass, the greater the stellar metallicity.

We note that in these 3D diagrams we have reduced the dimensionality of the problem, by considering the dependence of the stellar metallicity only on stellar and black hole mass. This means that the role of additional secondary parameters (SFR, ϕ_g, M_H, $(1+\delta)$) is somehow taken and embedded in the dependences on stellar and black hole mass, and this helps explain the fact that the partial correlation arrow and colour shading in Figure 2 does not exactly reproduce the (stronger) relative role of M_* and M_{BH} that one would expect from the random forest analysis (Fig.1).

The Black Hole-Metallicity Relation

Fig. 3 provides yet another visualisation of these relative dependencies, by showing 2D cuts of the 3D surface shown in Fig.2. Specifically, Fig. 3 shows the stellar metallicity versus black hole mass binned by tracks of stellar mass for star-forming (upper left) and passive (upper right) galaxies, and stellar metallicity versus stellar mass binned by tracks of black hole mass (lower left and right, same format). The upper figures show that, there is a tight correlation between stellar metallicity and black hole mass (BHZR) for passive galaxies, where the change in stellar mass between the tracks barely affects the relationship. On the contrary, for star-forming galaxies the change in stellar mass results in a significant offset of the tracks. The lower figures show that this is reversed for stellar metallicity versus stellar mass whilst binning in tracks of black hole mass. Summarising, for star forming galaxies at a given BH mass the metallicity depends strongly on stellar mass, while at a given stellar mass the stellar metallicity depends little on BH mass. These dependencies are swapped for passive galaxies: at a given BH mass the stellar metallicity does not depend on the stellar mass, while at any given stellar mass the stellar metallicity depends strongly on BH mass.

This result confirms that for star-forming galaxies we recover the standard MZR. However, for passive galaxies we find strong evidence for a Black Hole-Metallicity Relation (BHZR), between black hole mass and stellar metallicity.

We quantify this Black Hole-Metallicity Relation (BHZR) with the following linear fit in logarithmic quantities: $\log(\mathrm{Z}/\mathrm{Z}_\odot) = 0.106^{+0.031}_{-0.031}\,[\log(\mathrm{M_{BH}}/\mathrm{M}_\odot) - 8] + 0.106^{+0.033}_{-0.033}$ by using `LMFIT` [25]. Fig. 4 shows the best fit to the BHZR. We fit to the median bins of the BHZR so as to avoid being heavily biased by the overpopulated

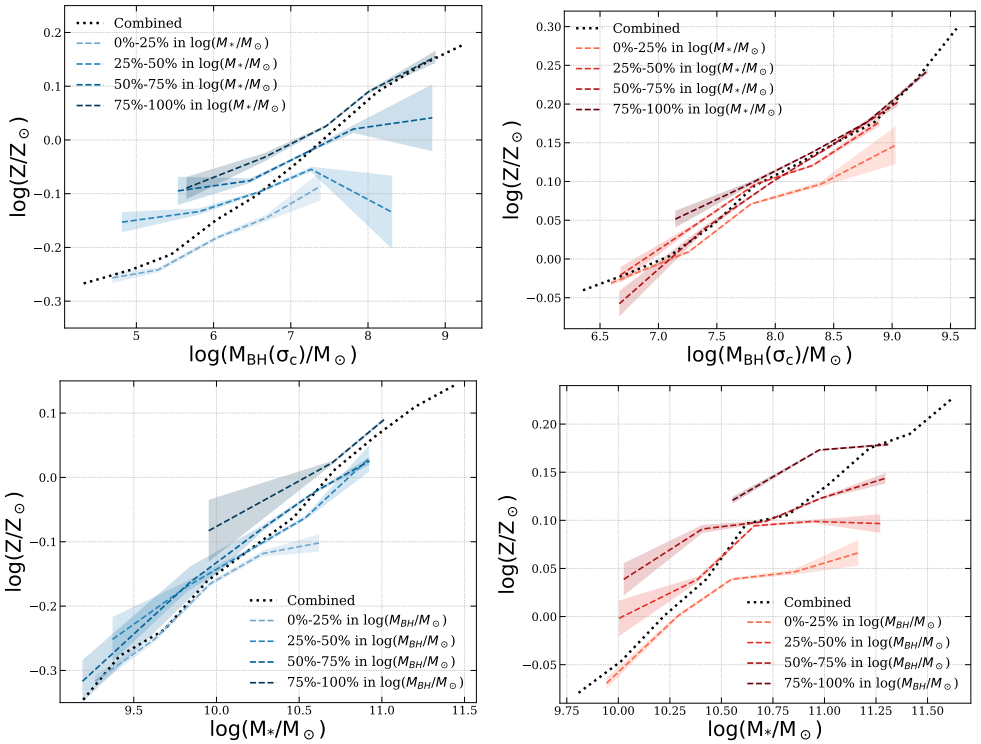

Fig. 3 Upper: stellar metallicity versus black hole mass binned by tracks of stellar mass for star-forming galaxies (left, blue) and passive galaxies (right, red). Lower: stellar metallicity versus stellar mass binned by tracks of black hole mass, again for star-forming (left, blue) and passive galaxies (right, red). The left hand plots show that the evolution in stellar metallicity for star-forming glaxies is primarily driven by stellar mass, whilst the right hand plots show that for passive galaxies the stellar metallicity is primarily driven by black hole mass.

centre of the contours. This means that according to the fit, a passive galaxy with $\log(\mathrm{M_{BH}/M_\odot}) = 8$ would be predicted to have stellar metallicity of $\log(\mathrm{Z/Z_\odot}) = 0.106$.

Is it black hole mass or gravitational potential?

One important consideration is to properly analyse whether σ_c is actually tracing black hole mass or is in fact tracing the dynamical mass or underlying gravitational potential. We conduct a test of this using ∼2000 galaxies from the MaNGA survey with accurate dynamical masses (for more details see section 1.2). We use two different samples of dynamical measurements. The first uses the dynamical masses from [26], which we also use to define the quantity $\phi_\mathrm{g} = \mathrm{M_{dyn}/r_e}$ (where r_e is the half-light radius), which is proportional to the gravitational potential. Fig. 5 upper panel shows the random forest regression results for these galaxies. We also use a similar sized sample of kinematic measurements from [27]. In this case the proxy for the (specific) gravitational potential is taken as the quantity $\phi_\mathrm{g} = \mathrm{V}^2 + 3\sigma^2$, where V is the rotation velocity and σ is the velocity dispersion. Fig. 5 lower panel shows the random forest

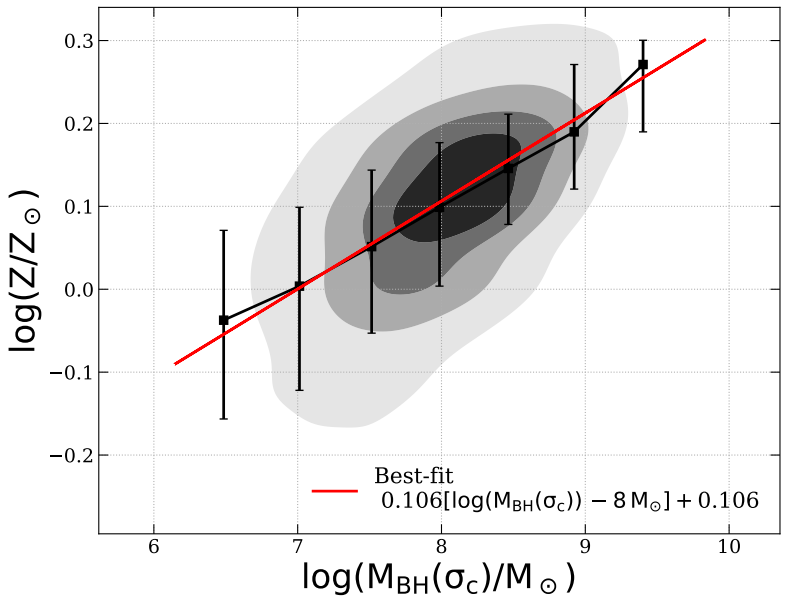

Fig. 4 Stellar metallicity versus black hole mass (as traced by central velocity dispersion) for passive galaxies. The outer density contour contains 90% of the galaxy population. The black squares show the median values in bins of black hole mass with the errorbars corresponding to the 16th and 84th percentiles of the distributions in each bin. The red line is the best-fit to these bins, showing the black hole metallicity relation (BHZR).

regression results for this sample of galaxies. The results for the two samples appear to agree, at least qualitatively. Essentially the star-forming sample shows a null result (although the stellar mass is still formally the most predictive quantity for the stellar metallicity), likely due to the small sample size of around 1000 galaxies, and in particular, the difficulty in measuring stellar metallicities for star-forming galaxies due to their weak stellar continuum and absorption lines. However, the key insight is from the passive sample. Clearly the black hole mass, as traced by σ_c, is the primary driver of the stellar metallicity, even with the addition of dynamical mass and both definitions of ϕ_g. This shows that the dependence seen on black hole mass (as traced by σ_c) is not a by product of a dependence on the gravitational potential or with the dynamical mass, rather it is actually direct dependence on black hole mass.

Summarising, the test performed in this section (although based on lower statistics than the SDSS DR7 sample), disfavours the scenario whereby the stellar metallicity dependence on black hole mass (via central velocity dispersion) is simply tracing deeper gravitational potentials in more massive galaxies. Rather this dependence is actually due to the black hole mass itself resulting from the integrated effect of AGN feedback.

Discussion

In summary, we have found that in star-forming galaxies the stellar metallicity is driven primarily by the stellar mass in the MZR. This is likely tracing the integral

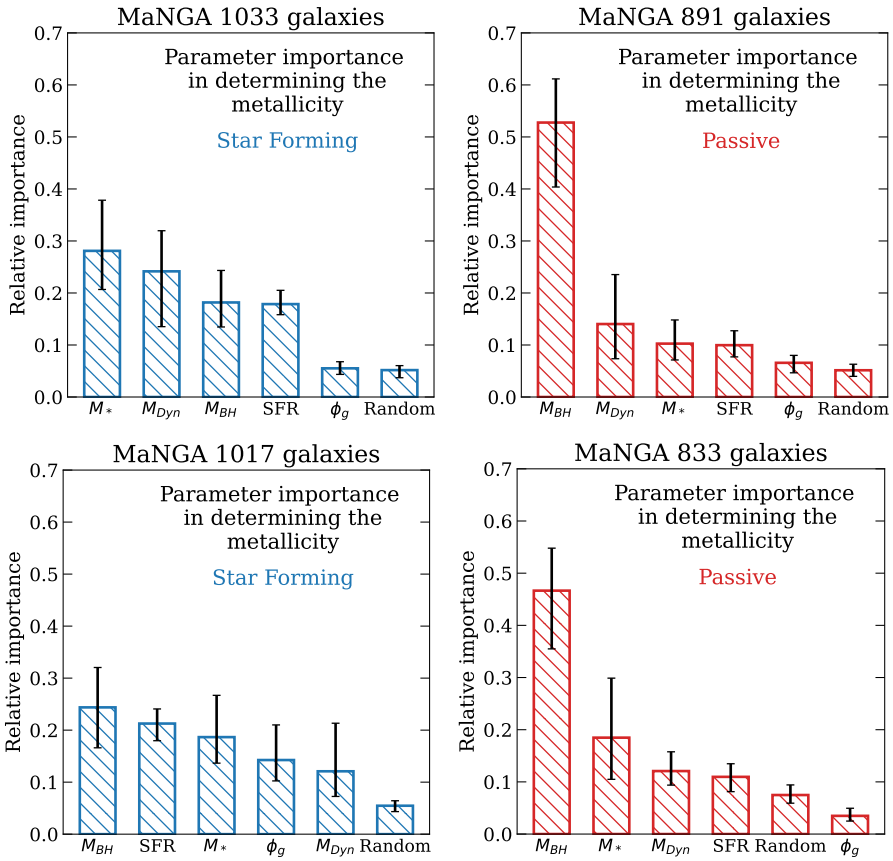

Fig. 5 Importance of various galactic properties in determining the stellar metallicity for star-forming (left panels) and passive (right panels) galaxies for two samples from the MaNGA survey ([26] top panels, [27] bottom panels), for which spatially resolved spectroscopy provides accurate dynamical masses and gravitational potentials. Left panels: star forming galaxies; right panels: passive galaxies. The following galactic parameters are considered: stellar mass (M_*), black hole mass as traced by σ_c, star formation rate (SFR), the dynamical mass, a control uniform random variable (Random), gravitational potential traced by $\phi_{\rm g} = {\rm M_{dyn}/r_e}$ and specific gravitational potential traced by $\phi_{\rm gs} = {\rm V}^2 + 3\sigma^2$. The left hand panels show that for star-forming galaxies there is no clear primary dependence for the stellar metallicity, due to a combination of a small sample size and difficulty accurately measuring stellar metallicities of star-forming galaxies. However, they key result is that for passive galaxies (right hand panels) the dependence is almost purely on black hole mass, even with the addition of the dynamical mass, and both definitions of the gravitational potential ϕ_g.

of metal formation (as seen for gas-phase metallicities in [19]): more massive galaxies have produced a greater mass of stars, hence a greater amount of metals. We also find a secondary dependence on SFR consistent with the FMR. However, we have discovered that for passive galaxies the stellar metallicity is driven primarily by black hole mass (as traced by σ_c) in a BHZR. The black hole mass provides an indication of the integrated history of feedback associated with black hole accretion, so this relation

Table 1 Number of galaxies contained within each SDSS sample once all cuts and matches have been made. Samples are star-forming stellar metallicities (SF Z sample) and non-star-forming stellar metallicities (NSF Z sample). Can see that there are many more passive galaxies than SF, hence the need to separate out these classes to properly explore the drivers.

	# of galaxies	$\log(M_*/M_\odot)$	$\log(\mathrm{SFR}/M_\odot \mathrm{yr})$	Overdensity
SF	16505	9.0 - 11.6	-1.0 - 1.5	-1.2 - 2.1
Q	37241	9.6 - 11.7	-2.1 - 0	-1.2 - 2.7

likely stems from the black hole quenching galaxies via halo heating (either preventative or delayed feedback), which suppresses gas accretion and results in 'starvation'. Residual star formation during starvation results in a rapid increase of metallicity as a consequence of closed box evolution without any diluting inflows.

This result crucially bridges the previous gap between studies of the stellar metallicities, finding evidence for starvation being a key quenching mechanism, and the causal relation between black hole mass and quenching.

1 Methods

1.1 SDSS Data

We use data about stellar masses and star-formation rates from the Sloan Digital Sky Survey (SDSS) data release 7 [20] MPA-JHU catalogue [4, 28]. We then match this catalogue to another used in [11], containing mass and light weighted stellar metallicities fitted by the spectral fitting code FireFly [29]. FIREFLY is a spectral fitting code that uses χ^2 minimization using a linear combination of simple stellar populations which vary in stellar ages and metallicities. The stellar population models used are those of [30] as well as input spectra from MILES [31] and a Kroupa IMF [32]. We also use mass-weighted halo masses and central satellite classifications from [33, 34], and overdensities from [35]. We also match to a catalogue of central velocity dispersions from the NYU value added catalogue [36]. We sigma clip the resulting dataset to 3σ to remove outliers that could bias the random forest or partial correlation coefficients. We show the resulting sample for SDSS in Table 2. This dataset enables us to explore the drivers of the stellar metallicity for a large number of galaxies (15,000+ in each sample) whilst also being able to explore many parameters of interest relating to each individual galaxy and its environment.

1.2 MaNGA Data

We also use data from the Mapping nearby Galaxies at Apache Point Observatory (MaNGA) Survey [23], which enables us to also include accurately measured dynamical masses from [26] and kinematic measurements from [27]. We use stellar metallicities, stellar masses and star-formation rates from [37, 38]. This significantly cuts down our sample statistics to around 1000 galaxies each for the star-forming and passive

Table 2 Table showing random forest regression hyper-parameters (from left to right), size of the test sample compared to training sample, the number of estimators, the minimum sample size at the end (leaf) node, the maximum depth of the decision trees, and the number of times the forest was bootstrapped for the percentiles.

	test_size	n_est	min_samp_leaf	max_depth	n_times	MSE test	MSE train
SDSS	50%	200	15	100	100	0.007	0.005
MaNGA	20%	200	15	100	100	0.008	0.005

samples, but enables us to control for these quantities which were unavailable in the larger SDSS sample.

1.3 Random Forest Regression

A random forest is a collection of many different decision trees each of which attempts to reduce a quantity called mean squared error (MSE, which itself measures the quality of each split) which enables it to calculate parameter importances in driving a target variable. We split the larger SDSS sample 50-50 into a training and test sample (we use an 80-20 split for the much smaller MaNGA samples to ensure a larger training set). The random forest is applied to the training sample to build a model which is then applied to the test sample to find the parameter importances. Errors for the parameter importances are calculated by bootstrap random sampling the random forest regression 100 times - we then take the 16th and 84th percentiles of the resulting distribution. We compare the test and training sample's mean squared errors (MSE) to ensure that the model is not overfitting. For the random forest regression for the passive galaxies (shown in the right panel of Fig. 1), we find a MSE of 0.007 for the testing sample and 0.005 for the training sample. For the star-forming galaxies, it is 0.017 and 0.013 respectively. This shows that there has been no significant overfitting or underfitting. One of the key benefits of random forest regression is that it can probe several intercorrelated parameters simultaneously (allowing us to investigate many parameters at once). It can also find non-monotonic relationships between them. Furthermore, random forests have been found previously to be able to find intrinsic dependencies among many intercorrelated variables [providing the quantity the target truly depends on is included, 15]. They have also been shown to be able to successfully reverse engineer simulations in [14, 15]. We include the random forest hyper-parameters and the passive galaxy sample mean squared errors of the test and training sample in Table 2.

1.4 Partial correlation coefficients

Partial correlation coefficients allow us to take the correlation between two quantities A and B whilst controlling for any further correlation with quantity C. This means that if A and C are truly correlated, and B has a correlation with C this correlation will not introduce a an unphysical observed correlation between A and B. This is important in determining whether relationships are intrinsic or stem from relationships

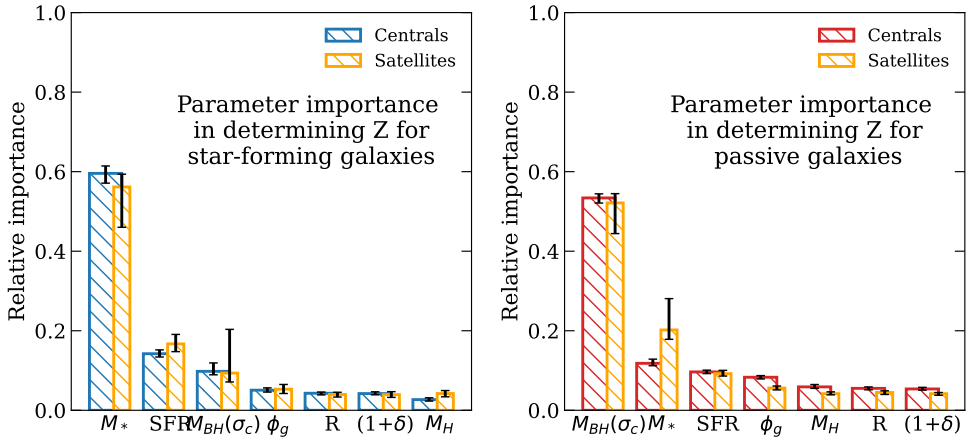

Fig. 6 The parameter importances of various galactic properties in determining the stellar metallicity (Z) for star-forming (left panel) and passive (right panel) galaxies, split into central (blue or red, wider bars) or satellite galaxies (orange, thinner bars) . The galactic parameters evaluated are stellar mass (M_*), star formation rate (SFR), black hole mass ($M_{\rm BH}$), the gravitational potential (ϕ_g), a control uniform random variable (Random), overdensities (1-δ), and halo mass (M_H). We see from both panels that there is little difference between centrals or satellites.

between other quantities that are not considered. We use partial correlation coefficients to determine the direction of any found relationship, i.e. as the random forest only gives us their importances, the PCCs can tell us whether two quantities correlate or anti-correlate. In addition to this it can provide an additional, although less powerful, method for checking the random forest results. The ratios of partial correlation coefficients can be used to define a gradient arrow on a 2D colour plot [17, 24]

$$\tan(\theta) = \frac{\rho_{\rm yz|x}}{\rho_{\rm xz|y}} \tag{1}$$

where θ is the arrow angle measured anticlockwise from the horizontal while $\frac{\rho_{\rm yz|x}}{\rho_{\rm xz|y}}$ is the ratio of the partial correlation coefficients between the y axis and colour-coded (z axis) quantities (whilst controlling for the x axis quantity), to the x axis and colour-coded (z axis) quantities (whilst controlling for the y axis quantity). The gradient arrow then points in the direction of the greatest increase in the colour-coded quantity - it enables the dependence of that quantity on the x and y axis quantities to be identified visually, whilst the angle of the arrow enables it to be determined quantitatively. As an example, If the x and y axis quantities contributed equally to determining the colour-coded quantity, we would expect an arrow angle of 45 degrees.

1.5 Centrals vs Satellites

We can explore whether these relations we have found are the same for central and satellite galaxies. This is another test of whether environment plays a significant role. The differences between the stellar metallicities of central and satellite galaxies have

been highlighted previously in [10]. We can probe whether this is the case by using our random forest regression methodology. The first stage is to split the dataset into central and satellite galaxies. We use a mass-weighted approach for this with central galaxies being classified as the most massive galaxy in their group [33, 34], with the remaining galaxies being classified as satellites. We also test using a light-weighted classification and find it makes no significant difference. Fig. 6 shows the random forest regression parameter importances, in exactly the same form as Fig. 1, only this time with the star-forming and passive samples split into central or satellite galaxies based upon whether they are the most massive galaxy in their group. We can see from Fig. 6 that the results remain the same regardless of central or satellite classification, i.e. again we find stellar metallicity is not driven by environmental effects. Interestingly this is different to what was found in [10], which we attribute to being able analyse almost all relevant parameters simultaneously with the random forest, which was not possible in the case of [10].

1.6 Reliability of σ as a tracer of black hole mass

Another question is exactly how reliable σ_c (the central stellar velocity dispersion) is as a tracer of black hole mass. This has previously been explored in [14], where they found that out of stellar mass, bulge mass and stellar velocity dispersion it was the stellar velocity dispersion that most tightly correlated with the black hole mass (as obtained from the directly measured black hole masses in [39]). Velocity dispersion has also been found to follow the local relation with black hole mass at higher redshifts [40] suggesting this is likely a universal relationship.

Acknowledgements

WB, RM, acknowledge support by the Science and Technology Facilities Council (STFC), by the ERC Advanced Grant 695671 'QUENCH', and by the UKRI Frontier Research grant RISEandFALL. RM also acknowledges funding from a research professorship from the Royal Society.

Availability of data and materials

The SDSS DR7 data is publicly available. The MaNGA data used is also publicly available.

Code availability

AstroPy [41], LMFIT [25] and FireFly [29] are publicly available.

References

[1] Maiolino, R., Mannucci, F.: De re metallica: the cosmic chemical evolution of galaxies. A&ARv **27**(1), 3 (2019) https://doi.org/10.1007/s00159-018-0112-2 arXiv:1811.09642 [astro-ph.GA]

[2] Origlia, L., Ranalli, P., Comastri, A., Maiolino, R.: Stellar and Gaseous Abundances in M82. ApJ **606**(2), 862–868 (2004) https://doi.org/10.1086/383018 arXiv:astro-ph/0401361 [astro-ph]

[3] Chisholm, J., Tremonti, C., Leitherer, C.: Metal-enriched galactic outflows shape the mass-metallicity relationship. MNRAS **481**(2), 1690–1706 (2018) https://doi.org/10.1093/mnras/sty2380 arXiv:1808.10453 [astro-ph.GA]

[4] Tremonti, C.A., Heckman, T.M., Kauffmann, G., Brinchmann, J., Charlot, S., White, S.D.M., Seibert, M., Peng, E.W., Schlegel, D.J., Uomoto, A., Fukugita, M., Brinkmann, J.: The Origin of the Mass-Metallicity Relation: Insights from 53,000 Star-forming Galaxies in the Sloan Digital Sky Survey. ApJ **613**(2), 898–913 (2004) https://doi.org/10.1086/423264 arXiv:astro-ph/0405537 [astro-ph]

[5] Zahid, H.J., Kudritzki, R.-P., Conroy, C., Andrews, B., Ho, I.-T.: Stellar Absorption Line Analysis of Local Star-forming Galaxies: The Relation between Stellar Mass, Metallicity, Dust Attenuation, and Star Formation Rate. ApJ **847**(1), 18 (2017) https://doi.org/10.3847/1538-4357/aa88ae arXiv:1708.07107 [astro-ph.GA]

[6] Mannucci, F., Cresci, G., Maiolino, R., Marconi, A., Gnerucci, A.: A fundamental relation between mass, star formation rate and metallicity in local and high-redshift galaxies. MNRAS **408**(4), 2115–2127 (2010) https://doi.org/10.1111/j.1365-2966.2010.17291.x arXiv:1005.0006 [astro-ph.CO]

[7] Baker, W.M., Maiolino, R., Belfiore, F., Curti, M., Bluck, A.F.L., Lin, L., Ellison, S.L., Thorp, M., Pan, H.-A.: The metallicity's fundamental dependence on both local and global galactic quantities. MNRAS **519**(1), 1149–1170 (2023) https://doi.org/10.1093/mnras/stac3594 arXiv:2210.03755 [astro-ph.GA]

[8] Looser, T., D'Eugenio, F.: The stellar Fundamental Metallicity Relation: the correlation between stellar mass, star-formation rate and stellar metallicity. ApJ, submitted (2023)

[9] Kumari, N., Maiolino, R., Belfiore, F., Curti, M.: Metallicity calibrations for diffuse ionized gas and low-ionization emission regions. MNRAS **485**(1), 367–381 (2019) https://doi.org/10.1093/mnras/stz366 arXiv:1902.01408 [astro-ph.GA]

[10] Peng, Y., Maiolino, R., Cochrane, R.: Strangulation as the primary mechanism for shutting down star formation in galaxies. Nat **521**(7551), 192–195 (2015) https://doi.org/10.1038/nature14439 arXiv:1505.03143 [astro-ph.GA]

[11] Trussler, J., Maiolino, R., Maraston, C., Peng, Y., Thomas, D., Goddard, D., Lian, J.: Both starvation and outflows drive galaxy quenching. MNRAS **491**(4), 5406–5434 (2020) https://doi.org/10.1093/mnras/stz3286 arXiv:1811.09283 [astro-ph.GA]

[12] Trussler, J., Maiolino, R., Maraston, C., Peng, Y., Thomas, D., Goddard, D., Lian, J.: The weak imprint of environment on the stellar populations of galaxies. MNRAS **500**(4), 4469–4490 (2021) https://doi.org/10.1093/mnras/staa3545 arXiv:2006.01154 [astro-ph.GA]

[13] Man, A., Belli, S.: Star formation quenching in massive galaxies. Nature Astronomy **2**, 695–697 (2018) https://doi.org/10.1038/s41550-018-0558-1 arXiv:1809.00722 [astro-ph.GA]

[14] Piotrowska, J.M., Bluck, A.F.L., Maiolino, R., Peng, Y.: On the quenching of star formation in observed and simulated central galaxies: evidence for the role of integrated AGN feedback. MNRAS **512**(1), 1052–1090 (2022) https://doi.org/10.1093/mnras/stab3673 arXiv:2112.07672 [astro-ph.GA]

[15] Bluck, A.F.L., Maiolino, R., Brownson, S., Conselice, C.J., Ellison, S.L., Piotrowska, J.M., Thorp, M.D.: The quenching of galaxies, bulges, and disks since cosmic noon. A machine learning approach for identifying causality in astronomical data. A&A **659**, 160 (2022) https://doi.org/10.1051/0004-6361/202142643 arXiv:2201.07814 [astro-ph.GA]

[16] Bluck, A.F.L., Piotrowska, J.M., Maiolino, R.: The Fundamental Signature of Star Formation Quenching from AGN Feedback: A Critical Dependence of Quiescence on Supermassive Black Hole Mass, Not Accretion Rate. ApJ **944**(1), 108 (2023) https://doi.org/10.3847/1538-4357/acac7c arXiv:2301.03677 [astro-ph.GA]

[17] Baker, W.M., Maiolino, R., Bluck, A.F.L., Lin, L., Ellison, S.L., Belfiore, F., Pan, H.-A., Thorp, M.: The ALMaQUEST survey IX: the nature of the resolved star forming main sequence. MNRAS **510**(3), 3622–3628 (2022) https://doi.org/10.1093/mnras/stab3672 arXiv:2201.03592 [astro-ph.GA]

[18] Baker, W.M., Maiolino, R., Belfiore, F., Bluck, A.F.L., Curti, M., Wylezalek, D., Bertemes, C., Bothwell, M.S., Lin, L., Thorp, M., Pan, H.-A.: The molecular gas main sequence and Schmidt-Kennicutt relation are fundamental, the star-forming main sequence is a (useful) byproduct. MNRAS **518**(3), 4767–4781 (2023) https://doi.org/10.1093/mnras/stac3413 arXiv:2211.10449 [astro-ph.GA]

[19] Baker, W.M., Maiolino, R.: Stellar mass, not dynamical mass nor gravitational potential, drives the mass-metallicity relationship. MNRAS (2023) https://doi.org/10.1093/mnras/stad802 arXiv:2303.08145 [astro-ph.GA]

[20] Abazajian, K.N., Adelman-McCarthy, J.K., Agüeros, M.A., Allam, S.S., Allende Prieto, C., An, D., Anderson, K.S.J., Anderson, S.F., Annis, J., Bahcall, N.A., Bailer-Jones, C.A.L., Barentine, J.C., Bassett, B.A., Becker, A.C., Beers, T.C., Bell, E.F., Belokurov, V., Berlind, A.A., Berman, E.F., Bernardi, M., Bickerton, S.J., Bizyaev, D., Blakeslee, J.P., Blanton, M.R., Bochanski, J.J., Boroski, W.N., Brewington, H.J., Brinchmann, J., Brinkmann, J., Brunner, R.J., Budavári, T., Carey, L.N., Carliles, S., Carr, M.A., Castander, F.J., Cinabro, D., Connolly,

A.J., Csabai, I., Cunha, C.E., Czarapata, P.C., Davenport, J.R.A., de Haas, E., Dilday, B., Doi, M., Eisenstein, D.J., Evans, M.L., Evans, N.W., Fan, X., Friedman, S.D., Frieman, J.A., Fukugita, M., Gänsicke, B.T., Gates, E., Gillespie, B., Gilmore, G., Gonzalez, B., Gonzalez, C.F., Grebel, E.K., Gunn, J.E., György, Z., Hall, P.B., Harding, P., Harris, F.H., Harvanek, M., Hawley, S.L., Hayes, J.J.E., Heckman, T.M., Hendry, J.S., Hennessy, G.S., Hindsley, R.B., Hoblitt, J., Hogan, C.J., Hogg, D.W., Holtzman, J.A., Hyde, J.B., Ichikawa, S.-i., Ichikawa, T., Im, M., Ivezić, Ž., Jester, S., Jiang, L., Johnson, J.A., Jorgensen, A.M., Jurić, M., Kent, S.M., Kessler, R., Kleinman, S.J., Knapp, G.R., Konishi, K., Kron, R.G., Krzesinski, J., Kuropatkin, N., Lampeitl, H., Lebedeva, S., Lee, M.G., Lee, Y.S., French Leger, R., Lépine, S., Li, N., Lima, M., Lin, H., Long, D.C., Loomis, C.P., Loveday, J., Lupton, R.H., Magnier, E., Malanushenko, O., Malanushenko, V., Mandelbaum, R., Margon, B., Marriner, J.P., Martínez-Delgado, D., Matsubara, T., McGehee, P.M., McKay, T.A., Meiksin, A., Morrison, H.L., Mullally, F., Munn, J.A., Murphy, T., Nash, T., Nebot, A., Neilsen, J. Eric H., Newberg, H.J., Newman, P.R., Nichol, R.C., Nicinski, T., Nieto-Santisteban, M., Nitta, A., Okamura, S., Oravetz, D.J., Ostriker, J.P., Owen, R., Padmanabhan, N., Pan, K., Park, C., Pauls, G., Peoples, J. John, Percival, W.J., Pier, J.R., Pope, A.C., Pourbaix, D., Price, P.A., Purger, N., Quinn, T., Raddick, M.J., Re Fiorentin, P., Richards, G.T., Richmond, M.W., Riess, A.G., Rix, H.-W., Rockosi, C.M., Sako, M., Schlegel, D.J., Schneider, D.P., Scholz, R.-D., Schreiber, M.R., Schwope, A.D., Seljak, U., Sesar, B., Sheldon, E., Shimasaku, K., Sibley, V.C., Simmons, A.E., Sivarani, T., Allyn Smith, J., Smith, M.C., Smolčić, V., Snedden, S.A., Stebbins, A., Steinmetz, M., Stoughton, C., Strauss, M.A., SubbaRao, M., Suto, Y., Szalay, A.S., Szapudi, I., Szkody, P., Tanaka, M., Tegmark, M., Teodoro, L.F.A., Thakar, A.R., Tremonti, C.A., Tucker, D.L., Uomoto, A., Vanden Berk, D.E., Vandenberg, J., Vidrih, S., Vogeley, M.S., Voges, W., Vogt, N.P., Wadadekar, Y., Watters, S., Weinberg, D.H., West, A.A., White, S.D.M., Wilhite, B.C., Wonders, A.C., Yanny, B., Yocum, D.R., York, D.G., Zehavi, I., Zibetti, S., Zucker, D.B.: The Seventh Data Release of the Sloan Digital Sky Survey. ApJS **182**(2), 543–558 (2009) https://doi.org/10.1088/0067-0049/182/2/543 arXiv:0812.0649 [astro-ph]

[21] Renzini, A., Peng, Y.-j.: An Objective Definition for the Main Sequence of Star-forming Galaxies. ApJ **801**(2), 29 (2015) https://doi.org/10.1088/2041-8205/801/2/L29 arXiv:1502.01027 [astro-ph.GA]

[22] Saglia, R.P., Opitsch, M., Erwin, P., Thomas, J., Beifiori, A., Fabricius, M., Mazzalay, X., Nowak, N., Rusli, S.P., Bender, R.: The SINFONI Black Hole Survey: The Black Hole Fundamental Plane Revisited and the Paths of (Co)evolution of Supermassive Black Holes and Bulges. ApJ **818**(1), 47 (2016) https://doi.org/10.3847/0004-637X/818/1/47 arXiv:1601.00974 [astro-ph.GA]

[23] Bundy, K., Bershady, M.A., Law, D.R., Yan, R., Drory, N., MacDonald, N., Wake, D.A., Cherinka, B., Sánchez-Gallego, J.R., Weijmans, A.-M., Thomas, D., Tremonti, C., Masters, K., Coccato, L., Diamond-Stanic, A.M., Aragón-Salamanca, A., Avila-Reese, V., Badenes, C., Falcón-Barroso, J., Belfiore, F.,

Bizyaev, D., Blanc, G.A., Bland-Hawthorn, J., Blanton, M.R., Brownstein, J.R., Byler, N., Cappellari, M., Conroy, C., Dutton, A.A., Emsellem, E., Etherington, J., Frinchaboy, P.M., Fu, H., Gunn, J.E., Harding, P., Johnston, E.J., Kauffmann, G., Kinemuchi, K., Klaene, M.A., Knapen, J.H., Leauthaud, A., Li, C., Lin, L., Maiolino, R., Malanushenko, V., Malanushenko, E., Mao, S., Maraston, C., McDermid, R.M., Merrifield, M.R., Nichol, R.C., Oravetz, D., Pan, K., Parejko, J.K., Sanchez, S.F., Schlegel, D., Simmons, A., Steele, O., Steinmetz, M., Thanjavur, K., Thompson, B.A., Tinker, J.L., van den Bosch, R.C.E., Westfall, K.B., Wilkinson, D., Wright, S., Xiao, T., Zhang, K.: Overview of the SDSS-IV MaNGA Survey: Mapping nearby Galaxies at Apache Point Observatory. ApJ **798**(1), 7 (2015) https://doi.org/10.1088/0004-637X/798/1/7 arXiv:1412.1482 [astro-ph.GA]

[24] Bluck, A.F.L., Maiolino, R., Sánchez, S.F., Ellison, S.L., Thorp, M.D., Piotrowska, J.M., Teimoorinia, H., Bundy, K.A.: Are galactic star formation and quenching governed by local, global, or environmental phenomena? MNRAS **492**(1), 96–139 (2020) https://doi.org/10.1093/mnras/stz3264 arXiv:1911.08857 [astro-ph.GA]

[25] Newville, M., Stensitzki, T., Allen, D.B., Ingargiola, A.: LMFIT: Non-Linear Least-Square Minimization and Curve-Fitting for Python. Zenodo (2014). https://doi.org/10.5281/zenodo.11813

[26] Li, H., Mao, S., Cappellari, M., Ge, J., Long, R.J., Li, R., Mo, H.J., Li, C., Zheng, Z., Bundy, K., Thomas, D., Brownstein, J.R., Roman Lopes, A., Law, D.R., Drory, N.: SDSS-IV MaNGA: global stellar population and gradients for about 2000 early-type and spiral galaxies on the mass-size plane. MNRAS **476**(2), 1765–1775 (2018) https://doi.org/10.1093/mnras/sty334 arXiv:1802.01819 [astro-ph.GA]

[27] Brownson, S., Bluck, A.F.L., Maiolino, R., Jones, G.C.: What drives galaxy quenching? A deep connection between galaxy kinematics and quenching in the local Universe. MNRAS **511**(2), 1913–1941 (2022) https://doi.org/10.1093/mnras/stab3749 arXiv:2201.02484 [astro-ph.GA]

[28] Brinchmann, J., Charlot, S., White, S.D.M., Tremonti, C., Kauffmann, G., Heckman, T., Brinkmann, J.: The physical properties of star-forming galaxies in the low-redshift Universe. MNRAS **351**(4), 1151–1179 (2004) https://doi.org/10.1111/j.1365-2966.2004.07881.x arXiv:astro-ph/0311060 [astro-ph]

[29] Wilkinson, D.M., Maraston, C., Goddard, D., Thomas, D., Parikh, T.: FIREFLY (Fitting IteRativEly For Likelihood analYsis): a full spectral fitting code. MNRAS **472**(4), 4297–4326 (2017) https://doi.org/10.1093/mnras/stx2215 arXiv:1711.00865 [astro-ph.GA]

[30] Maraston, C., Strömbäck, G.: Stellar population models at high spectral resolution. MNRAS **418**(4), 2785–2811 (2011) https://doi.org/10.1111/j.1365-2966.2011.19738.x arXiv:1109.0543 [astro-ph.CO]

[31] Sánchez-Blázquez, P., Peletier, R.F., Jiménez-Vicente, J., Cardiel, N., Cenarro, A.J., Falcón-Barroso, J., Gorgas, J., Selam, S., Vazdekis, A.: Medium-resolution Isaac Newton Telescope library of empirical spectra. MNRAS **371**(2), 703–718 (2006) https://doi.org/10.1111/j.1365-2966.2006.10699.x arXiv:astro-ph/0607009 [astro-ph]

[32] Kroupa, P.: On the variation of the initial mass function. MNRAS **322**(2), 231–246 (2001) https://doi.org/10.1046/j.1365-8711.2001.04022.x arXiv:astro-ph/0009005 [astro-ph]

[33] Yang, X., Mo, H.J., van den Bosch, F.C., Jing, Y.P.: A halo-based galaxy group finder: calibration and application to the 2dFGRS. MNRAS **356**(4), 1293–1307 (2005) https://doi.org/10.1111/j.1365-2966.2005.08560.x arXiv:astro-ph/0405234 [astro-ph]

[34] Yang, X., Mo, H.J., van den Bosch, F.C., Pasquali, A., Li, C., Barden, M.: Galaxy Groups in the SDSS DR4. I. The Catalog and Basic Properties. ApJ **671**(1), 153–170 (2007) https://doi.org/10.1086/522027 arXiv:0707.4640 [astro-ph]

[35] Peng, Y.-j., Lilly, S.J., Kovač, K., Bolzonella, M., Pozzetti, L., Renzini, A., Zamorani, G., Ilbert, O., Knobel, C., Iovino, A., Maier, C., Cucciati, O., Tasca, L., Carollo, C.M., Silverman, J., Kampczyk, P., de Ravel, L., Sanders, D., Scoville, N., Contini, T., Mainieri, V., Scodeggio, M., Kneib, J.-P., Le Fèvre, O., Bardelli, S., Bongiorno, A., Caputi, K., Coppa, G., de la Torre, S., Franzetti, P., Garilli, B., Lamareille, F., Le Borgne, J.-F., Le Brun, V., Mignoli, M., Perez Montero, E., Pello, R., Ricciardelli, E., Tanaka, M., Tresse, L., Vergani, D., Welikala, N., Zucca, E., Oesch, P., Abbas, U., Barnes, L., Bordoloi, R., Bottini, D., Cappi, A., Cassata, P., Cimatti, A., Fumana, M., Hasinger, G., Koekemoer, A., Leauthaud, A., Maccagni, D., Marinoni, C., McCracken, H., Memeo, P., Meneux, B., Nair, P., Porciani, C., Presotto, V., Scaramella, R.: Mass and Environment as Drivers of Galaxy Evolution in SDSS and zCOSMOS and the Origin of the Schechter Function. ApJ **721**(1), 193–221 (2010) https://doi.org/10.1088/0004-637X/721/1/193 arXiv:1003.4747 [astro-ph.CO]

[36] Blanton, M.R., Schlegel, D.J., Strauss, M.A., Brinkmann, J., Finkbeiner, D., Fukugita, M., Gunn, J.E., Hogg, D.W., Ivezić, Ž., Knapp, G.R., Lupton, R.H., Munn, J.A., Schneider, D.P., Tegmark, M., Zehavi, I.: New York University Value-Added Galaxy Catalog: A Galaxy Catalog Based on New Public Surveys. AJ **129**(6), 2562–2578 (2005) https://doi.org/10.1086/429803 arXiv:astro-ph/0410166 [astro-ph]

[37] Sánchez, S.F., Pérez, E., Sánchez-Blázquez, P., González, J.J., Rosáles-Ortega, F.F., Cano-Díaz, M., López-Cobá, C., Marino, R.A., Gil de Paz, A., Mollá, M., López-Sánchez, A.R., Ascasibar, Y., Barrera-Ballesteros, J.: Pipe3D, a pipeline to analyze Integral Field Spectroscopy Data: I. New fitting philosophy of FIT3D. RMXAA **52**, 21–53 (2016) https://doi.org/10.48550/arXiv.1509.08552

arXiv:1509.08552 [astro-ph.IM]

[38] Sánchez, S.F., Pérez, E., Sánchez-Blázquez, P., García-Benito, R., Ibarra-Mede, H.J., González, J.J., Rosales-Ortega, F.F., Sánchez-Menguiano, L., Ascasibar, Y., Bitsakis, T., Law, D., Cano-Díaz, M., López-Cobá, C., Marino, R.A., Gil de Paz, A., López-Sánchez, A.R., Barrera-Ballesteros, J., Galbany, L., Mast, D., Abril-Melgarejo, V., Roman-Lopes, A.: Pipe3D, a pipeline to analyze Integral Field Spectroscopy Data: II. Analysis sequence and CALIFA dataproducts. RMXAA **52**, 171–220 (2016) https://doi.org/10.48550/arXiv.1602.01830 arXiv:1602.01830 [astro-ph.IM]

[39] Terrazas, B.A., Bell, E.F., Woo, J., Henriques, B.M.B.: Supermassive Black Holes as the Regulators of Star Formation in Central Galaxies. ApJ **844**(2), 170 (2017) https://doi.org/10.3847/1538-4357/aa7d07 arXiv:1707.01097 [astro-ph.GA]

[40] Maiolino, R., Scholtz, J., Curtis-Lake, E., Carniani, S., Baker, W., de Graaff, A., Tacchella, S., Übler, H., D'Eugenio, F., Witstok, J., Curti, M., Arribas, S., Bunker, A.J., Charlot, S., Chevallard, J., Eisenstein, D.J., Egami, E., Ji, Z., Jones, G.C., Lyu, J., Rawle, T., Robertson, B., Rujopakarn, W., Perna, M., Sun, F., Venturi, G., Williams, C.C., Willott, C.: JADES. The diverse population of infant Black Holes at 4¡z¡11: merging, tiny, poor, but mighty. arXiv e-prints, 2308–01230 (2023) https://doi.org/10.48550/arXiv.2308.01230 arXiv:2308.01230 [astro-ph.GA]

[41] Astropy Collaboration, Price-Whelan, A.M., Lim, P.L., Earl, N., Starkman, N., Bradley, L., Shupe, D.L., Patil, A.A., Corrales, L., Brasseur, C.E., Nöthe, M., Donath, A., Tollerud, E., Morris, B.M., Ginsburg, A., Vaher, E., Weaver, B.A., Tocknell, J., Jamieson, W., van Kerkwijk, M.H., Robitaille, T.P., Merry, B., Bachetti, M., Günther, H.M., Aldcroft, T.L., Alvarado-Montes, J.A., Archibald, A.M., Bódi, A., Bapat, S., Barentsen, G., Bazán, J., Biswas, M., Boquien, M., Burke, D.J., Cara, D., Cara, M., Conroy, K.E., Conseil, S., Craig, M.W., Cross, R.M., Cruz, K.L., D'Eugenio, F., Dencheva, N., Devillepoix, H.A.R., Dietrich, J.P., Eigenbrot, A.D., Erben, T., Ferreira, L., Foreman-Mackey, D., Fox, R., Freij, N., Garg, S., Geda, R., Glattly, L., Gondhalekar, Y., Gordon, K.D., Grant, D., Greenfield, P., Groener, A.M., Guest, S., Gurovich, S., Handberg, R., Hart, A., Hatfield-Dodds, Z., Homeier, D., Hosseinzadeh, G., Jenness, T., Jones, C.K., Joseph, P., Kalmbach, J.B., Karamehmetoglu, E., Kałuszyński, M., Kelley, M.S.P., Kern, N., Kerzendorf, W.E., Koch, E.W., Kulumani, S., Lee, A., Ly, C., Ma, Z., MacBride, C., Maljaars, J.M., Muna, D., Murphy, N.A., Norman, H., O'Steen, R., Oman, K.A., Pacifici, C., Pascual, S., Pascual-Granado, J., Patil, R.R., Perren, G.I., Pickering, T.E., Rastogi, T., Roulston, B.R., Ryan, D.F., Rykoff, E.S., Sabater, J., Sakurikar, P., Salgado, J., Sanghi, A., Saunders, N., Savchenko, V., Schwardt, L., Seifert-Eckert, M., Shih, A.Y., Jain, A.S., Shukla, G., Sick, J., Simpson, C., Singanamalla, S., Singer, L.P., Singhal, J., Sinha, M., Sipőcz, B.M., Spitler, L.R., Stansby, D., Streicher, O.,

Šumak, J., Swinbank, J.D., Taranu, D.S., Tewary, N., Tremblay, G.R., de Val-Borro, M., Van Kooten, S.J., Vasović, Z., Verma, S., de Miranda Cardoso, J.V., Williams, P.K.G., Wilson, T.J., Winkel, B., Wood-Vasey, W.M., Xue, R., Yoachim, P., Zhang, C., Zonca, A., Astropy Project Contributors: The Astropy Project: Sustaining and Growing a Community-oriented Open-source Project and the Latest Major Release (v5.0) of the Core Package. ApJ **935**(2), 167 (2022) https://doi.org/10.3847/1538-4357/ac7c74 arXiv:2206.14220 [astro-ph.IM]